

FULL PAPER

hERG stereoselective modulation by mexiletine-derived ureas: Molecular docking study, synthesis, and biological evaluation

Gualtiero Milani¹ | Roberta Budriesi² | Elisa Tavazzani³ |
Maria Maddalena Cavalluzzi¹  | Laura Beatrice Mattioli² |
Daniela Valeria Miniero⁴ | Pietro Delre^{5,6} | Benny Danilo Belviso⁶  |
Marco Denegri³ | Corrado Cuocci⁶ | Natalie Paola Rotondo¹ |
Annalisa De Palma⁴ | Roberta Galdani⁷ | Rocco Caliandro⁶ |
Giuseppe Felice Mangiatordi⁶ | Amit Kumawat⁸ | Carlo Camilloni⁸ |
Silvia Priori^{3,9,10} | Giovanni Lentini¹ 

¹Department of Pharmacy—Pharmaceutical Sciences, University of Bari Aldo Moro, Bari, Italy

²Department of Pharmacy and Biotechnology, Food Chemistry and Nutraceutical Lab, Alma Mater Studiorum-University of Bologna, Bologna, Italy

³ICS-Maugeri IRCCS, Pavia, Italy

⁴Department of Biosciences, Biotechnologies, and Environment, University Aldo Moro of Bari, Bari, Italy

⁵Chemistry Department, University of Bari Aldo Moro, Bari, Italy

⁶CNR—Institute of Crystallography, Bari, Italy

⁷Institute of Neuroscience, Université Catholique de Louvain, Brussels, Belgium

⁸Department of Biosciences, University of Milan, Milano, Italy

⁹Molecular Cardiology, Department of Molecular Medicine, University of Pavia, Pavia, Italy

¹⁰Centro Nacional de Investigaciones Cardiovasculares Carlos III, Madrid, Spain

Correspondence

Maria Maddalena Cavalluzzi, Department of Pharmacy—Pharmaceutical Sciences, University of Bari Aldo Moro, via E. Orabona n. 4, 70126 Bari, Italy.

Email: mariamaddalena.cavalluzzi@uniba.it

Funding information

Fondazione Telethon—Italy,
Grant/Award Number: # GGP19134

Abstract

Long QT syndrome (LQTS) is a disorder of cardiac electrophysiology resulting in life-threatening arrhythmias; nowadays, only a few drugs are available for the management of LQTS. Focusing our attention on LQT2, one of the most common subtypes of LQTS caused by mutations in the human ether-à-go-go-related gene (*hERG*), in the present work, the stereoselectivity of the recently discovered mexiletine-derived urea **8** was investigated on the hERG potassium channel. According to preliminary *in silico* predictions, *in vitro* studies revealed a stereoselective behavior, with the *meso* form showing the greatest hERG opening activity. In addition, functional studies on guinea pig isolated left atria, aorta, and

Gualtiero Milani, Roberta Budriesi, and Elisa Tavazzani contributed equally as first authors.

Silvia Priori and Giovanni Lentini contributed equally as senior authors.

This is an open access article under the terms of the Creative Commons Attribution License, which permits use, distribution and reproduction in any medium, provided the original work is properly cited.

© 2023 The Authors. *Archiv der Pharmazie* published by Wiley-VCH GmbH on behalf of Deutsche Pharmazeutische Gesellschaft.

ileum demonstrated that **8** does not present any cardiac or intestinal liability in our ex vivo studies. Due to its overall profile, (*R,S*)-**8** paves the way for the design and development of a new series of compounds potentially useful in the treatment of both congenital and drug-induced forms of LQTS.

KEYWORDS

hERG channels, long QT syndrome, mexiletine, molecular docking, ureas

1 | INTRODUCTION

Urea represents a privileged structure in drug design and development, providing potent drug–target interactions by forming multiple stable hydrogen bonds with proteins. Therefore, a wide range of biologically active urea-based compounds has been developed over the last few years, including anticancer, antibacterial, anticonvulsant, antiviral, anti-inflammatory, and antidiabetic agents.^[1–8] Some compounds containing the urea scaffold have also been approved by Food and Drug Administration (FDA) (Figure 1), including the ergot-related dopamine agonist lisuride used in the treatment of Parkinson's disease, the atypical antipsychotic cariprazine used in schizophrenia and bipolar disorders, the NS3/4A protease inhibitor boceprevir useful against hepatitis C virus (HCV),^[1] and the anticancer agents sorafenib, lenvatinib, and regorafenib, approved for the treatment of advanced hepatocellular carcinoma (HCC).^[1,9–11] On the other hand, some urea-based small molecules have also been proposed as human ether-à-go-go-related gene (hERG) potassium channel activators (NS1643 and NS3623) which accelerate myocardial repolarization by increasing the outward potassium current during the ventricular action potential.^[12,13] Therefore, they are potentially useful for the treatment of both congenital and drug-induced forms of long QT syndrome (LQTS),^[12] a cardiovascular disorder characterized by abnormal cardiac repolarization, leading to a prolonged QT interval and T-wave irregularities on the surface electrocardiogram (ECG), and responsible for a concomitant risk of *Torsade de Pointes*, a well-known potentially life-threatening arrhythmia.^[14,15] Starting from the consideration that mexiletine—a well-known voltage-gated sodium channel blocking agent clinically useful as class Ib antiarrhythmic and antimyotonic agent^[16–20]—can reverse the action potential prolongation in patients with LQTS,^[21–26] and in analogy with the urea-based hERG potassium channel activators, we recently described an asymmetric mexiletine urea [(*R,R*)-1,3-bis[1-(2,6-dimethylphenoxy)propan-2-yl]urea, MC450, Figure 1], which shared some structure and electrophysiological features with the “Type 2” activators of the hERG potassium channel.^[27]

It mainly acts on the inactivation mechanism of the channel unlike “Type 1” activators that slow the rate of channel deactivation. The mechanism of action of MC450 is similar to that described for the two previously reported ureas NS-1643 and NS-3623, thus corroborating the role of the urea scaffold as a useful chemotype in the quest for hERG openers.^[28]

Starting from the observation that the hERG channel is involved in cardiac disorders and very few and even old studies have been devoted to the evaluation of the cardiac activity of urea-based compounds so far,^[29–35] we aimed to explore the cardiovascular effect of MC450, together with its *SS* enantiomer and the *RS* (*meso*) form to gain insight on a possible stereoselective behavior. These compounds were prepared in high optical purity by an alternative and more efficient stereospecific route than what was previously reported for the *RR* enantiomer.^[27] Their respective chemical and optical purity were checked through a chiral high performance liquid chromatography (HPLC) method and crystal structures were determined by the X-ray crystallography.

2 | RESULTS AND DISCUSSION

2.1 | Chemistry

Despite our previously reported accidental synthesis of (*R,R*)-**8**,^[27] the desired optically active urea has been firstly synthesized by a convergent synthesis reported in Scheme 1.

The amino group of commercial (*R*)-alaninol [(*R*)-**1**] was tert-Butyloxycarbonyl (BOC)-protected^[36] and the so-obtained *N*-BOC alaninol [(*R*)-**2**] was reacted with 2,6-dimethylphenol under Mitsunobu conditions.^[19] Deprotection of aryl alkyl ether (*R*)-**3** with trifluoroacetic acid gave (*R*)-mexiletine [(*R*)-**4**]. In parallel, the carboxylic acid (*R*)-**7** was prepared as previously reported.^[18] By reacting (*R*)-**4** and (*R*)-**7** according to the Curtius rearrangement, urea (*R,R*)-**8** was finally obtained. However, this method gave the desired product [(*R,R*)-**8**] in low overall yield (8%). Thus, a shorter and more efficient procedure was then developed (Scheme 2), by modifying a literature procedure.^[37] Once obtained (*R*)-mexiletine as described in Scheme 1, it was reacted with half an equivalent of 1,1'-carbonyldiimidazole (CDI) in MeCN to give urea (*R,R*)-**8** with 78% overall yield. This procedure, with minor modifications (see Section 4), was then successfully applied to the preparation of the *SS*-enantiomer [(*SS*)-**8**] and the *meso* form [(*RS*)-**8**] for whose synthesis (*S*)-mexiletine was prepared according to the same synthetic route depicted for the enantiomer in Scheme 1, starting from (*S*)-alaninol. The ee values were >99.5% for both enantiomers, as shown by chiral HPLC (Supporting Information: Figures S1 and S2).

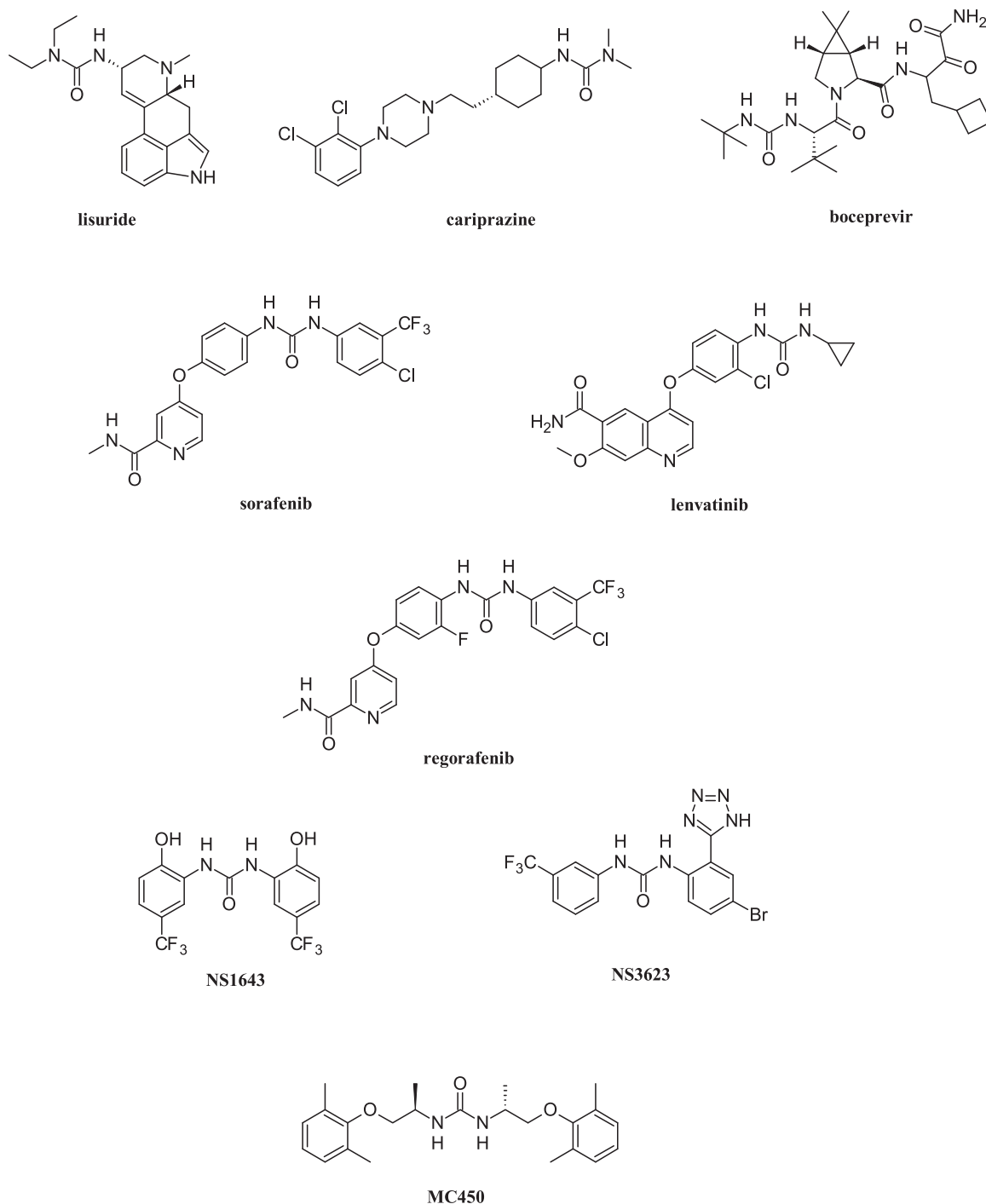


FIGURE 1 Structures of the Food and Drug Administration (FDA)-approved drugs lisuride, cariprazine, boceprevir, sorafenib, lenvatinib, and regorafenib; the human ether-à-go-go-related gene (hERG) agonists NS1643 and NS3623; the mexiletine urea MC450.

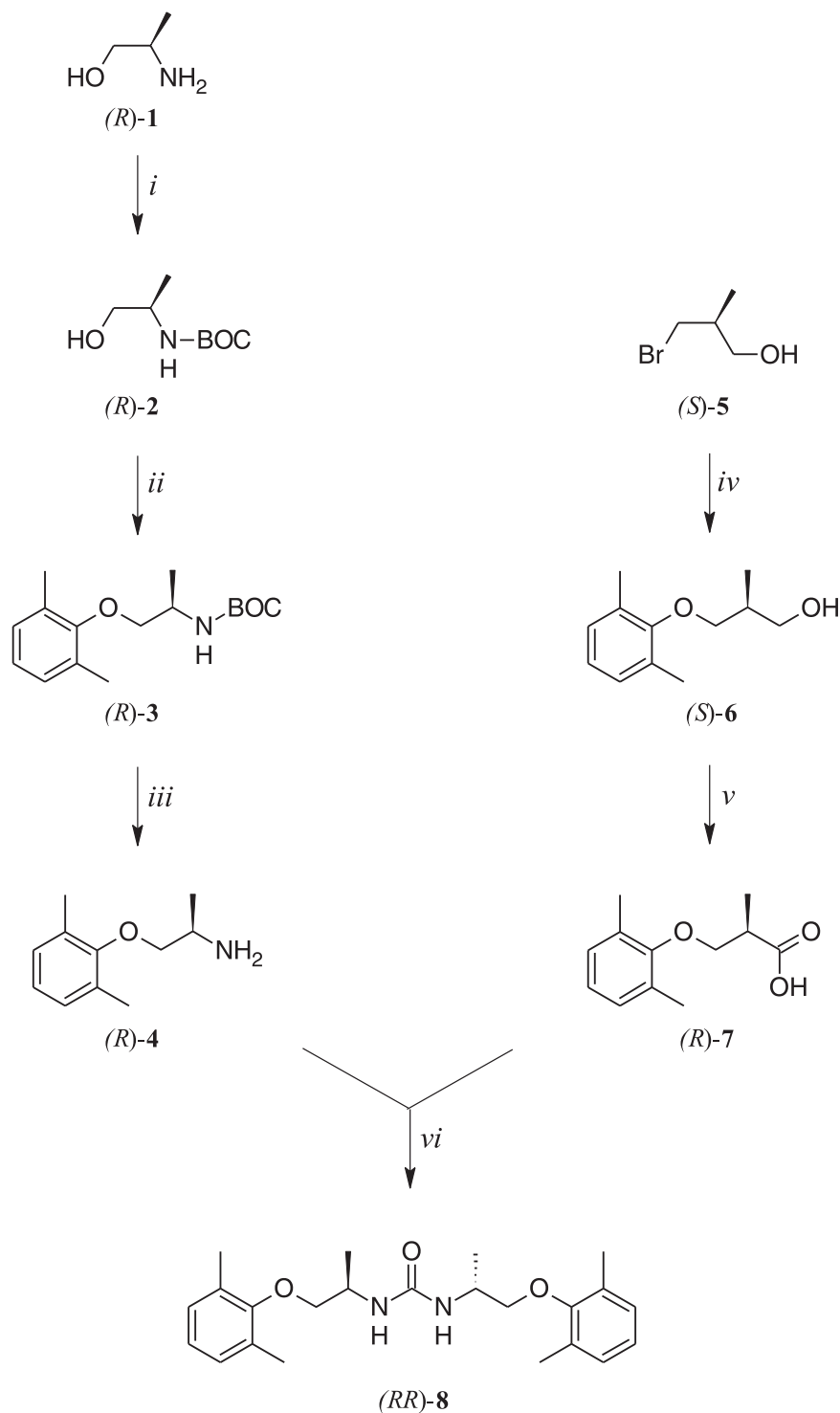
2.2 | Crystal structure determination

Being known the dependence of the *E/Z* conformation equilibrium on the pattern of *N*-substitution in ureas,^[38,39] the crystal structures of (*S,S*)-**8** and (*R,S*)-**8** were determined by X-ray diffraction powder data to confirm the *Z,Z* conformation to support molecular docking simulation study. A real-space method based on the simulated annealing algorithm (SA) was used and the crystal cell and symmetry

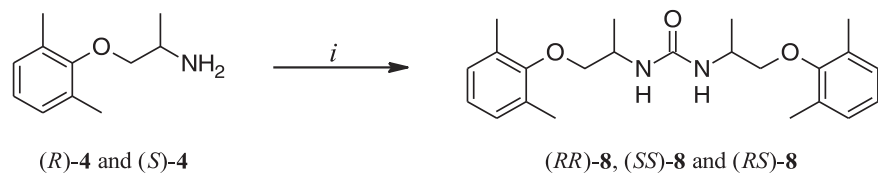
were determined by an automatic analysis of the diffraction profile (Supporting Information: Table S1).

The crystal structures of the individual molecules and their crystal packing are shown in Figure 2, while crystal data and refinement parameters are reported in Supporting Information: Table S1.

The analysis of crystal packing (Figure 2c,d) highlights common intermolecular contacts for (*S,S*)-**8** and (*R,S*)-**8**: (i) the carbamide



SCHEME 1 Synthesis of (RR)-8. Reagents and conditions: (i) BOC_2O , 1 M NaOH, THF, room temp.; (ii) 2,6-dimethylphenol, diisopropyl azodicarboxylate, triphenylphosphine, anhyd THF, room temp.; (iii) CF_3COOH , room temp.; (iv) 2,6-dimethylphenol, NaH 60%, DMF, 0°C; (v) RuO_2 , 10% NaIO_4 , EtOAc, room temp.; (vi) DPPA, triethylamine, dioxane, 90°C.



SCHEME 2 Synthesis of (RR)-8, (SS)-8, and (RS)-8. Reagents and conditions: (a) CDI, CH_3CN , room temp.

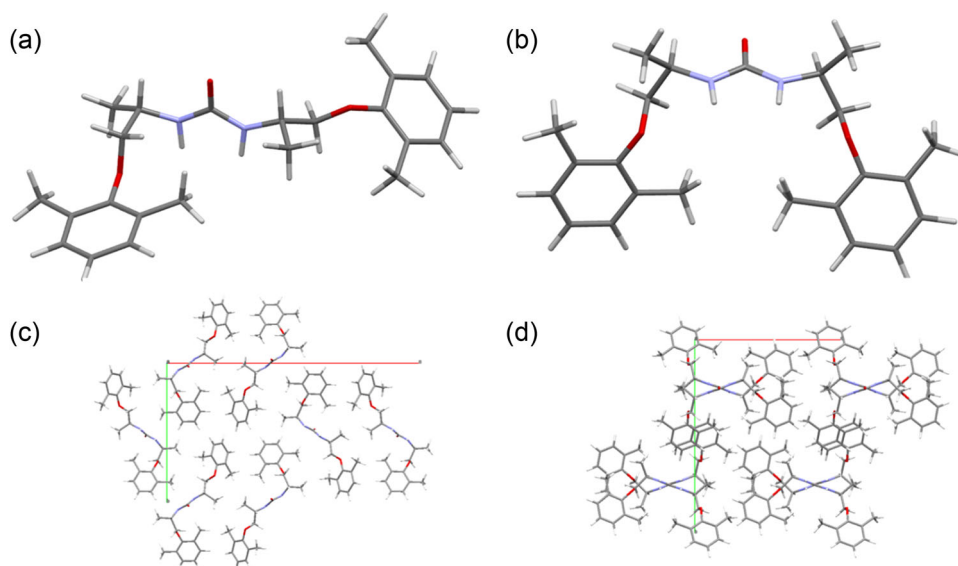


FIGURE 2 Crystal structures of (S,S)-8 (a, c) and (R,S)-8 (b, d). (a, b) Asymmetric unit with color legend: carbon (light gray), hydrogen (white), oxygen (red), nitrogen (blue). (c, d) Packing in the crystal cell, where all hydrogen atoms have been removed for clarity. The unit cell of both molecules is shown in perspective view along the *c*-axis.

oxygen atom is involved in hydrogen bonds with each of the two carbamide nitrogen atoms belonging to a symmetry-related molecule. For such interactions, the H–O distances range from 1.9 Å to 2.1 Å and the NH–O angles range from 148° to 158°, as expected for moderate hydrogen bonds.^[40] (ii) Molecules in the crystal are stacked along the shorter unit cell axis (c). Such stacking could be ascribed to π – π interactions among the aromatic moieties of the molecules in the crystal, although the observed ring-to-ring distances (4.5–6.5 Å) are larger than those expected for such interactions.^[41] The aromatic moieties involved in π – π interactions show a parallel-displaced geometry, as a result of the attractive interaction between one of the methyl groups bound to phenyl and the phenyl group of a symmetry-related molecule.

Despite the relative position of the methyl and phenyl group being similar for both the molecules under investigation, (S,S)-8 shows shorter ring-to-ring distances than (R,S)-8, suggesting a stronger stacking interaction in this case.

2.3 | Molecular docking

LQT2, one of the most frequent subtypes of congenital LQTS, is associated with mutations in genes encoding hERG and is related to the loss of function of the channel.^[42] In 2017, we reported on the discovery of MC450 (Figure 1), a new mexiletine-derived opener of the hERG K⁺ channel able to shorten action potential duration, thus having therapeutic potential for the treatment of LQT2. Although this compound could exist in three different stereoisomers, only the isolated RR enantiomer [(R,R)-8] was at first evaluated as a hERG opener. Based on the interesting obtained results, in-depth studies on the SS enantiomer [(S,S)-8] and the *meso* form [(R,S)-8] would be

advisable as well. Therefore, a preliminary *in silico* investigation on a possible stereoselective behavior has been performed on the recently published cryo-EM structure of the human ERG (hERG) channel (pdb code: 5VA1). Notably, ligand-induced fit effects were included during the simulations, as proved to be of utmost importance for obtaining reliable docking data on the available hERG protein structures.^[43] Figure 3 shows the obtained top-scored docking poses. Remarkably, (R,R)-8 and (R,S)-8 share a very similar binding mode where the urea moiety is crucial to engage a dual well-oriented H-bond with the sidechain of S631(D). In addition, molecular recognition seems to be the result of favorable hydrophobic interactions/contacts with N633(D), N588(C), and G628 (D). A different binding mode is instead returned by (S,S)-8 which is predicted to engage an H-bond interaction with the backbone of G628 (B) (via its urea moiety) and hydrophobic interactions with G628 (D) and N588 (B). The picture that emerged from this analysis indicates that (R,R)-8 and (R,S)-8 fit better than (S,S)-8 in the hERG binding site. This seems to be the result of a better orientation of the urea scaffold allowing the establishment of a well-oriented dual H-bond interaction with the protein cavity. Interestingly, the computed binding free energies are in agreement with the performed visual inspection, with (R,R)-8 and (R,S)-8 outperforming (S,S)-8 in terms of molecular mechanics/generalized Born surface area (molecular mechanics/generalized Born surface area [MM-GBSA]) score (60.3 and 58.9 kcal/mol vs. 45.7 kcal/mol). These data, taken as a whole, support the hypothesis, which is consistent with the available literature,^[44,45] whereby the hERG molecular recognition might be stereoselective, and underline the importance of S631 and G628 in the interaction between hERG and urea-based activators. Note that this hypothesis is in full agreement with the experimental literature displaying that the hERG double mutant G628C/S631C is insensitive to (R,R)-8.^[27]

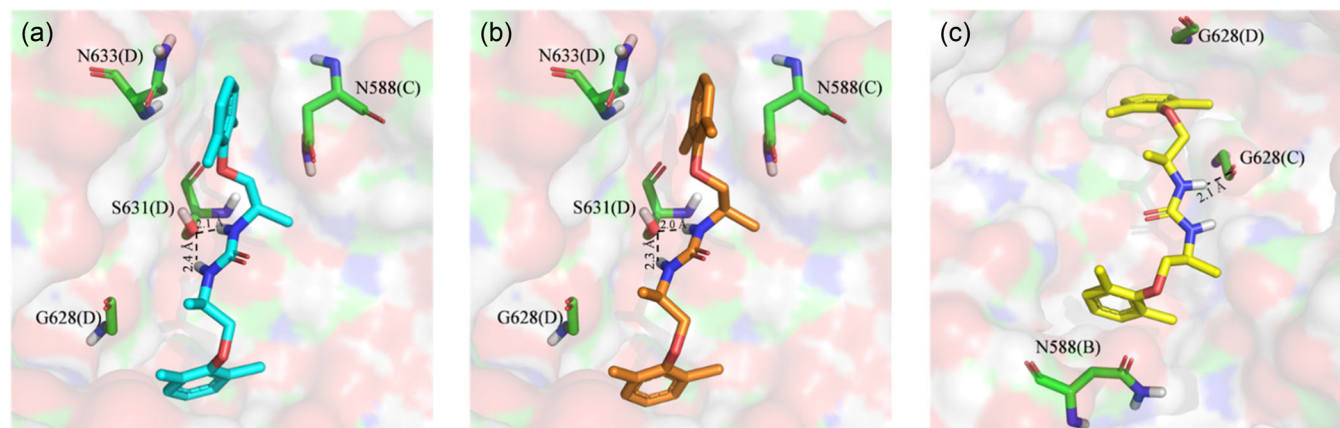


FIGURE 3 Top-scored docking poses of (a) *(R,R)*-8, (b) *(R,S)*-8, and (c) *(S,S)*-8 within the human ether-à-go-go-related gene (hERG) binding site. Ligands and important residues are rendered as sticks, whereas the protein is represented as a surface. H-bonds are represented by dotted black lines. For the sake of clarity, only polar hydrogen atoms are shown.

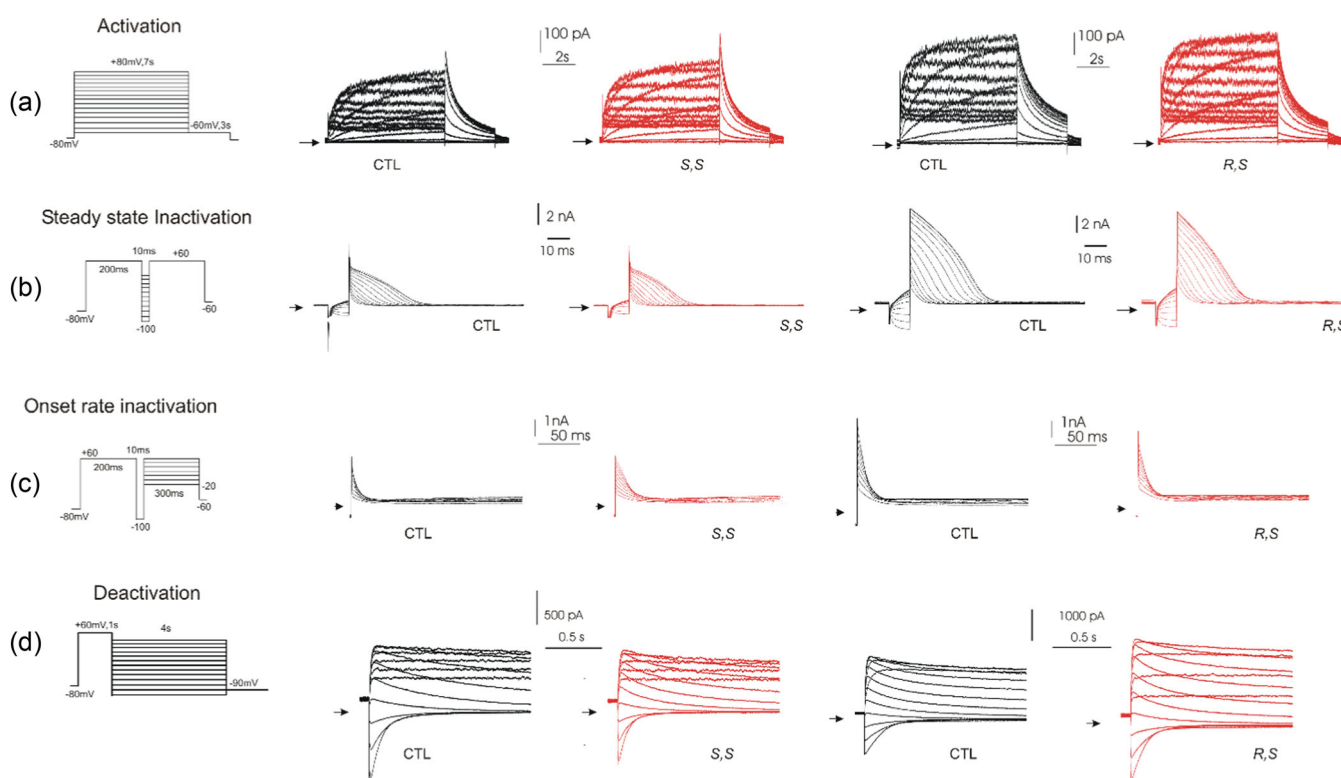


FIGURE 4 Voltage clamp recordings of human ether-à-go-go-related gene (hERG) currents in HEK cells. The currents were elicited in HEK cells by the protocol indicated on the left of the figure (a–d). On the right, the recorded currents are reported in the control condition (CTL, in black) and after the perfusion of 25 μ M of the compound of interest (*(S,S)*-8 or *(R,S)*-8 in red. The arrows indicate the zero-current level.

2.4 | Pharmacology

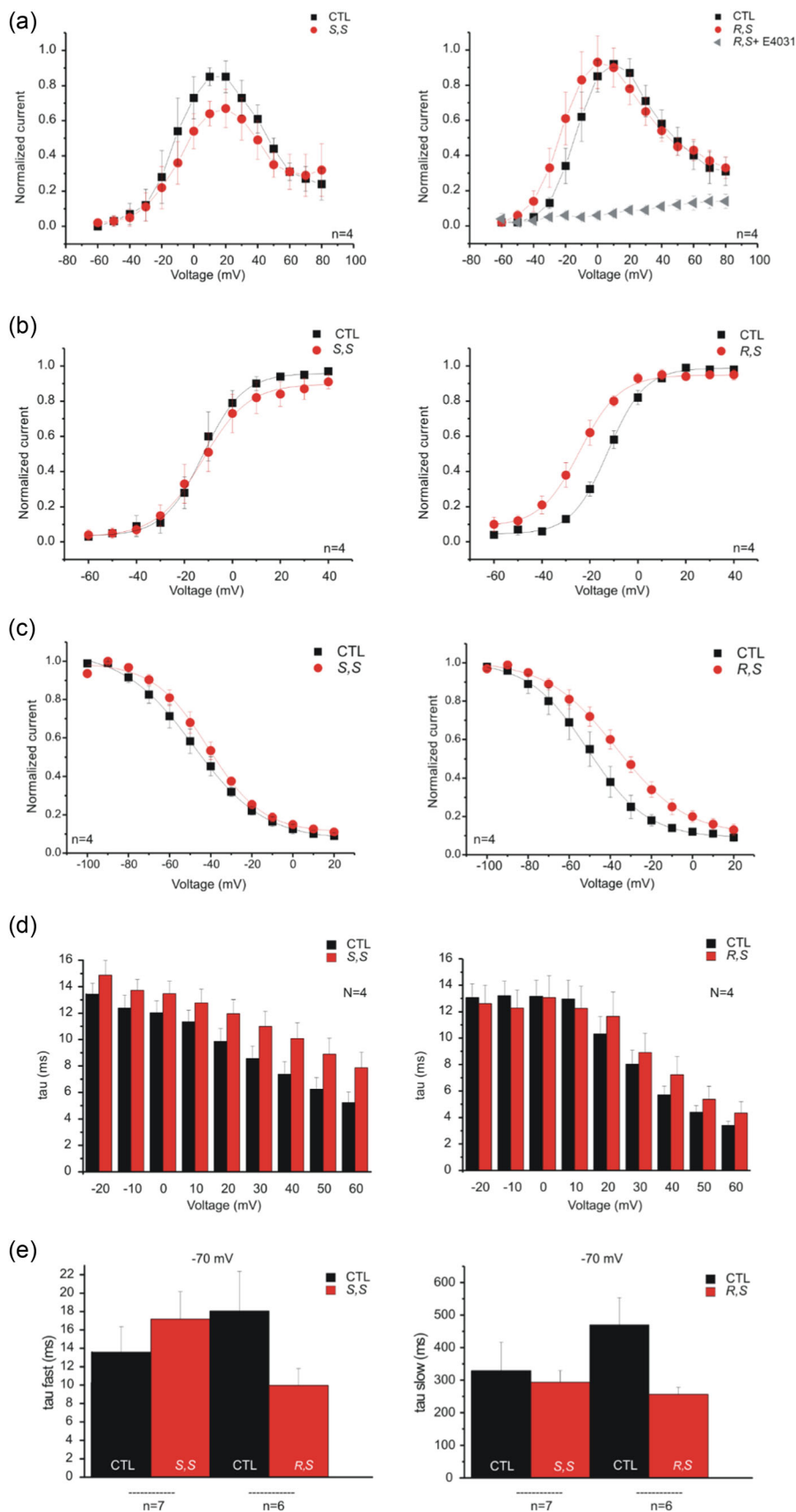
2.4.1 | hERG binding activity

The newly synthesized *(S,S)*-8 and *(R,S)*-8 were tested on hERG wild-type channels. In particular, the effect of each compound was evaluated on the activation (Figures 4a and 5a,b), inactivation

(Figures 4b,c and 5c,d) and deactivation (Figures 4d and 5e) of I_{Kr} flowing through the hERG channel expressed in human embryonic kidney (HEK) cells.

- **Activation.** To study the activation and assess if the newly synthesized *(S,S)*-8 and *(R,S)*-8 influence the bell-shaped I/V relationship of hERG and avoid undermining the half point for the

FIGURE 5 Electrophysiological investigations in HEK cells expressing human ether-à-go-go-related gene (hERG) channels. Black squares indicate the value of current in basal condition (control = CTL) and the red dots indicate the values of current after the perfusion of 25 μ M of the indicated compound (a–c). The I/V plots represent the steady-state activation currents (a), peak activation currents (b), and the steady-state inactivation currents (c). The gray triangles indicated the effect of (R,S)-8 on the steady-state current under the block of E4031 (50 nM). The histograms shown in (d) and (e) indicate the values of time constant in basal conditions (control = CTL, black columns) and after the perfusion of 25 μ M of the indicated compound (red columns), for the inactivation and deactivation phase, respectively. In all panels is reported the number of cells for the single investigation and the standard error bar.



channel activation ($V_{0.5}$), a double pulses protocol was employed. The hERG activation currents were determined by a holding potential of -80 mV, where the activation gate is closed and the channel is in its stable nonconducting state. Then, to allow activation to reach as close as possible to the steady state, the cells were stepped by pulses between -60 and $+80$ mV for 7 s. Then, currents were repolarized to more hyperpolarized potentials at -60 mV (for 3 s) to generate deactivating tail currents whose amplitude is related to the proportion of channel recovering from inactivation. The recorded currents (examples in Figure 4a) were measured at the end of the 7 s pulse (steady-state currents), were normalized to the maximal evoked current, and graphed as a function of the voltage used to build the steady-state activation I/V plot (Figure 5). The hERG steady-state current increases progressively and then slowly decreases to more positive voltage values, indicating that the voltage-dependent inactivation behavior characteristic of hERG current (control [CTL]) is maintained after the perfusion with the SS or RS isomers. The *S,S* isomer decreases the outward currents, and *(R,S)*-**8** induces a right shift in the steady-state curve without distorting particularly the bell-shaped curve. To investigate the possible effect of *(R,S)*-**8** on the pharmacologically induced LQTS, the inhibitor E4031 (50 nM) was perfused. By comparing the I/V plot of steady-state currents of *(R,S)*-**8** versus *(R,S)*-**8**+E4031 (Figure 5a), a statistical difference from -20 to $+80$ mV ($p < 0.05$) was revealed. To study the voltage dependence of activation, we analyzed the peak tail current amplitude that is elicited by a single potential (-60 mV) and reflects the proportion of channels activated during the previous depolarizing pulse (Figure 4a). The peak currents were normalized to the maximal evoked current and graphed as a function of the voltage used; the activation curve was fitted with a sigmoidal Boltzmann function (Figure 5b). The peak activation current of *(R,S)*-**8**, differently from *(S,S)*-**8**, shows statistically significant effect in comparison with the control conditions CTL: $V_{0.5} = -12.19 \pm 2.30$, $k = 8.30 \pm 1.45$ versus *(S,S)*-**8**: $V_{0.5} = -12.45 \pm 3.24$, $k = 9.59 \pm 2.39$; CTL: $V_{0.5} = -12.34 \pm 1.00$ mV, $k = 7.62 \pm 0.59$ versus *(R,S)*-**8**: $V_{0.5} = -24.09 \pm 2.05$, $k = 8.32 \pm 1.32$ ($p < 0.05$).

- **Inactivation.** A three steps protocol was used to investigate the steady-state inactivation (Figures 4b and 5c): after the application of a holding potential of -80 mV, the cells were depolarized at $+60$ mV for 200 ms to ensure the full inactivation of the hERG channel, then repolarized from -100 mV to $+20$ mV for 10 ms and repolarized at $+60$ mV for 200 ms. The currents evoked at this last pulse were measured and normalized to the maximum current and fitted with the sigmoidal Boltzmann function (Figure 5c) (CTL: $V_{0.5} = -48.37 \pm 0.6$, $k = 17.20 \pm 0.68$ vs *(S,S)*-**8**: $V_{0.5} = -41.28 \pm 1.03$, $k = 13.27 \pm 1.00$; CTL: $V_{0.5} = -50.96 \pm 0.6$, $k = 14.4 \pm 0.59$ vs *(R,S)*-**8**: $V_{0.5} = -37.06 \pm 0.75$, $k = 17.11 \pm 0.81$). This analysis was carried out to compare the perturbing effect of SS and RS on hERG current versus the control conditions. There is a statistically significant difference for the treatment with *(S,S)*-**8** ($p < 0.05$) from -80 mV, for CTL versus *(R,S)*-**8** ($p < 0.05$) from -60 to 0 mV ($p < 0.05$). To investigate more in deep the inactivation phase, we have studied the

onset rate of inactivation by using a three-pulses voltage clamp protocol shown in Figure 4c. Depolarizing pulse at $+60$ mV for 200 ms was employed to inactivate the channel, then a hyperpolarizing pulse at -100 mV for 10 ms was used to allow inactivation recovery, and finally, pulses between $+60$ and -20 mV (300 ms) elicited the outward inactivating currents (Figure 4c). Inactivation currents were fitted by a single exponential function to obtain the time constants (τ). The mean τ values are represented by the histograms in Figure 5d. No statistically significant differences were observed in the slowed inactivation kinetics.

- **Deactivation.** To determine the rates of deactivation of SS and RS on the hERG channel we used a two-step voltage protocol to elicit tail currents that were fitted by a biexponential function. Starting from a holding potential of -80 mV, the deactivation kinetics (Figures 4d and 5e) were examined in the voltage range from -100 to -20 mV after a depolarizing step at $+60$ mV to activate the hERG channel. During the second pulse phase, a growth of current is visible as the hERG channel recovers quickly from inactivation and then follows a current decay as the channel deactivates. The time course of the deactivating currents was fitted with a double exponential function to obtain the fast and slow time constants (τ) at -70 mV pulse. There is a statistically significant difference for CTL versus RS τ slow ($p < 0.05$).

Summing up these findings, *(RS)*-**8** shows a negative shift in the inactivation as previously reported for the RR enantiomer, and the SS enantiomer was the less potent stereoisomer, according to the in silico predictions. The different binding modes returned by *(S,S)*-**8** docking simulations are probably responsible for the impaired ability to activate the channel while allowing it to act with the same mechanism of action as the other two isomers. Overall, we can state that the urea of mexiletine (**8**) retains the hERG opening activity of the parent compound and that the stereoselective behavior observed in our study confirms the stereoselectivity of binding reported in the literature for the hERG channel.^[44]

Notably, both the tested stereoisomers proved to have mixed mechanisms by combining properties of the different types of the hERG potassium channel activators. Considering that Type 2 activators have been reported as drugs with a risk of repolarization overcorrection that could itself be pro-arrhythmic,^[46,47] unlike Type 1 activators,^[48,49] the observed mixed mechanism suggests a safer cardiac profile for the most potent RS isomer compared with both the previously reported RR enantiomer and the other Type 2 activators reported in the literature.

2.4.2 | Functional studies on cardiac parameters and smooth muscle function

To evaluate possible undesired effects, our compounds were tested in functional studies to evaluate their cardiac and vascular activities.

TABLE 1 Antiarrhythmic activity of tested compounds.

Compd	Max % increase of threshold of ac-arrhythmia after pretreatment with compounds ^a (M ± SEM)	EC ₅₀ ^b (μM)	95% conf. lim. (× 10 ⁻⁶)
Mexiletine	64 ± 1.4 ^c	11.61	8.71–13.47
(R,R)-8	10 ± 0.3 ^d	–	–
(S,S)-8	11 ± 0.4	–	–
(R,S)-8	3 ± 0.1	–	–

^aIncrease of the threshold of ac-arrhythmia: increase in the current strength of 50 Hz alternating current required to produce arrhythmia in guinea pig left atria driven at 1 Hz in the presence of each tested compound at 5×10^{-5} M. The 5×10^{-5} M concentration gave the maximum effect for most compounds.

^bCalculated from log concentration-response curves (Probit analysis according to Litchfield and Wilcoxon^[50] with $n = 6-8$). When the maximum effect was <50%, the EC₅₀ values were not calculated.

^cAt 10^{-4} M.

^dAt 10^{-5} M.

First of all, the three urea stereoisomers were in vitro tested for their antiarrhythmic activity on guinea pig isolated left atria driven at 1 Hz. The results were reported in Table 1 along with data for mexiletine taken as a reference compound. None of the stereoisomers increased the threshold of ac-arrhythmia, with the intrinsic activities being at the most 11%: such a mild effect was observed that the EC₅₀ values were not determined. Looking at the flip side, being known that hERG agonists are associated with a substantial risk of proarrhythmia,^[13,46,47] no arrhythmogenic effect was observed, this result highlighting the inability of our compounds to alter cardiac rhythm as a side effect.

Both negative inotropic and chronotropic activities of the three stereoisomers under evaluation were then determined, obtaining dose-response curves, and the results were reported in Table 2 along with the data for mexiletine. Unlike the latter, which showed quite similar negative inotropic and chronotropic effects, compounds (R,R)-, (S,S)-, and (R,S)-8 showed an interesting selective negative inotropic effect, also on the spontaneously beating right atrium, being devoid of the chronotropic one. Their chronotropic intrinsic activity does not exceed 33%, thus confirming the previously discussed lack of the arrhythmogenic effect. It is noteworthy that the negative inotropic effect on the spontaneously beating right atrium was not recorded for mexiletine since this insignificant inotropic effect mainly results from the chronotropic effect. Furthermore, the selectivity for cardiac inotropism allows us to speculate about the possible preferential binding of our compounds with the Cav1.2 subtype, mainly involved in cardiomyocyte contractility, rather than Cav1.3, responsible for chronotropy.^[51] It is noteworthy that the most interesting hERG opener (R,S)-8 displayed an inotropic EC₅₀ value higher than that of the RR and SS isomers and even one order of magnitude higher than that of mexiletine on the left atrium thus possibly acting as the safest stereoisomer in terms of cardiac profile. All compounds were also tested on K⁺-depolarized (80 mM KCl) guinea pig aortic strips (Table 3) and none of them displayed significant vascular effect, with the intrinsic vasorelaxant activity percentage on the aorta being lower than 30%, thus confirming a safe cardiovascular profile.

Finally, being known the undesired spasmolytic effect of Ca²⁺ channel antagonists, the activity on K⁺-depolarized (80 mM KCl)

guinea pig ileum smooth muscle was evaluated (Table 3), with the meso form [(R,S)-8] being devoid of possible intestinal side effects.

Unexpectedly, the results obtained so far pointed to possible off-target pharmacological activities for the RR isomer. It was the most potent negative inotrope stereoisomer with an EC₅₀ value of 8.5 nM on the left atria. (R,R)-8 was 3.9- and 48-fold more potent than (S,S)-8 and (R,S)-8, respectively, and about fivefold more potent than mexiletine. A greater inotropic potency of (R,R)-8 on right atria in the spontaneous activity was also established, with its EC₅₀ value being 0.10 μM in comparison to 0.38 and 0.62 μM of (S,S)-8 and (R,S)-8, respectively. Furthermore, since no effect on the aorta was observed, it displayed a remarkable selectivity for cardiac functional parameters compared with vascular ones. Furthermore, when tested on the ileum smooth muscle, it displayed an IC₅₀ value very close to the EC₅₀ value determined on the left atrium, thus leading to some considerations: (1) a possible L-type calcium channel-mediated activity could be responsible for the observed inotropic activity, (2) the RR isomer could also be suggested as a possible spasmolytic agent,^[52] (3) more in-depth studies aimed at the dissociation of the two observed pharmacological activities are required and will hereafter be carried out.

Figure 6 illustrates the above considerations by comparing the potencies of mexiletine and its urea stereoisomers. The figure clearly shows the negative inotropic effect observed for all compounds, the selectivity of (R,S)-8 with respect to mexiletine, and the highest potency of (S,S)-8 both on the isolated guinea-pig left atrium and on ileum.

2.5 | Cytotoxicity

The cytotoxic effect was assessed by the 3-(4,5-dimethylthiazol-2-yl)-2,5-diphenyltetrazolium bromide (MTT) test (Figure 7) on the human neuroblastoma (SH-SY5Y) cell line which was used to predict possible neural toxicity of our compounds being known that mexiletine clinical use is often associated with CNS toxicity.^[16,19]

Mexiletine was found to be nontoxic, showing an IC₅₀ value >100 μM, which is consistent with its current use as a drug. The IC₅₀

TABLE 2 Effects of the tested compounds on cardiac parameters.

Compd	Left atrium driven at 1 Hz Negative inotropy			Right atrium in spontaneously activity Negative inotropy			Negative chronotropy		
	Activity ^a (M ± S.E.M.)	EC ₅₀ ^b (μM)	95% conf lim (× 10 ⁻⁶)	Activity ^c (M ± S.E.M.)	EC ₅₀ ^b (μM)	95% conf lim (× 10 ⁻⁶)	Activity ^d (M ± S.E.M.)	EC ₅₀ ^b (μM)	95% conf lim (× 10 ⁻⁶)
Mexiletine	90 ± 1.3	0.045	0.035–0.058	n.d.	n.d.	n.d.	85 ± 2.6 ^h	0.028	0.023–0.035
(R,R)-8	89 ± 2.2 ^e	0.0085	0.0060–0.012	62 ± 2.3	0.10	0.075–0.14	33 ± 1.6 ^f	-	-
(S,S)-8	62 ± 3.2 ^f	0.033	0.028–0.052	51 ± 0.3 ^g	0.38	0.25–0.61	12 ± 0.6 ^f	-	-
(R,S)-8	57 ± 1.4	0.41	0.33–0.48	55 ± 1.4 ^g	0.62	0.46–0.84	5 ± 0.2	-	-

^aDecrease in developed tension on isolated guinea pig left atrium at 10⁻⁵ M, expressed as percent changes from the control (n = 5–6). The 10⁻⁵ M concentration gave the maximum effect for most compounds.
^bCalculated from log concentration-response curves (Probit analysis by Litchfield and Wilcoxon^[50] with n = 6–7). When the maximum effect was <50%, the EC₅₀ inotropic and EC₅₀ chronotropic values were not calculated.

^cDecrease in developed tension on guinea pig spontaneously beating isolated right atrium at 10⁻⁵ M, expressed as percent changes from the control (n = 7–8). The 10⁻⁵ M concentration gave the maximum effect for most compounds.

^dDecrease in atrial rate on guinea pig spontaneously beating isolated right atrium at 5 × 10⁻⁵ M, expressed as percent changes from the control (n = 7–8). The 10⁻⁵ M concentration gave the maximum effect for most compounds. Pretreatment heart rate ranged from 165 to 190 beats/min.

^eAt 10⁻⁶ M.

^fAt 5 × 10⁻⁶ M.

^gAt 5 × 10⁻⁵ M.

^hAt 10⁻⁷ M.

TABLE 3 Activity of tested compounds on K⁺-depolarized guinea pig smooth muscle.

Comp	Aorta			Ileum		
	Activity ^a (M ± SEM)	IC ₅₀ ^b (μM)	95% conf lim (× 10 ⁻⁶)	Activity ^a (M ± SEM)	IC ₅₀ ^b (μM)	95% conf lim (× 10 ⁻⁶)
Mexiletine	5 ± 0.3 ^c	-	-	81 ± 1.9 ^c	8.52	6.54–11.02
(R,R)-8	10 ± 1.6	-	-	95 ± 1.6 ^d	0.0080	0.0036–0.017
(S,S)-8	25 ± 1.4	-	-	62 ± 1.1	1.94	1.54–2.44
(R,S)-8	1 ± 0.3	-	-	33 ± 1.7	-	-

^aPercent inhibition of calcium-induced contraction on K⁺-depolarized (80 mM) guinea pig nonvascular (ileum) and vascular (aorta) smooth muscle at 5 × 10⁻⁵ M. The 5 × 10⁻⁵ M concentration gave the maximum effect for most compounds.

^bCalculated from log concentration-response curves (Probit analysis by Litchfield and Wilcoxon^[50] with *n* = 6–7). When the maximum effect was <50%, the IC₅₀ values were not calculated.

^cAt 10⁻⁴ M.

^dAt 5 × 10⁻⁸ M.

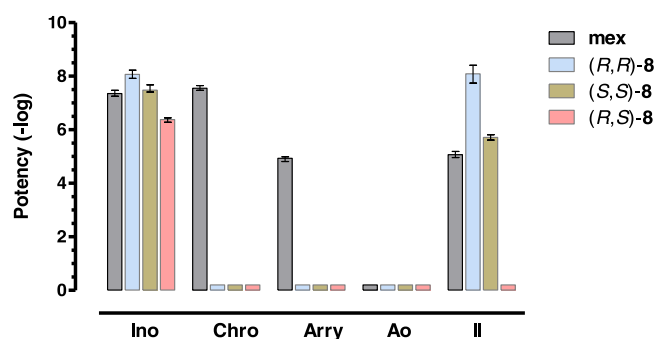


FIGURE 6 Each bar represents the $-\log EC_{50}$ obtained from 6 to 8 independent experiments. When bar errors are not shown, they are covered by the corresponding points. Ino, inotropy; Chro, chronotropy; Arry, antiarrhythmic activity; Ao, aorta; II, ileum.

values obtained for (R,R)-8, (S,S)-8, and (R,S)-8 were 72 ± 4 μM, >100 μM, and 52 ± 2 μM, respectively. Notably, the cytotoxicity of (R,R)-8 was observed at concentrations remarkably higher than those responsible for the negative inotropic effect (3–5 orders of magnitude), thus highlighting a safe profile for this compound. Concerning the RS isomer, the cytotoxic IC₅₀ value was only twofold higher than the concentration used to investigate its hERG agonism. However, further electrophysiological investigations on (R,S)-8 as an hERG opener at concentrations lower than those so far explored could be carried out to look for a wider gap between active and possibly toxic concentrations.

3 | CONCLUSIONS

In summary, in the present work, we report on the stereoselective behavior of the mexiletine-derived symmetric and asymmetric urea **8** as an hERG opener, with its cardiovascular profile having also been determined. Electrophysiological investigations in HEK cells expressing hERG channels demonstrated that the *meso* form (R,S)-8 is the most potent activator of the hERG potassium channel among

the three possible urea stereoisomers. The induced increase in the repolarizing potassium current could be helpful for the treatment of the LQTS since it could induce an action potential shortening. In addition, functional studies on guinea pig isolated left atria and aorta demonstrated its safe cardiovascular profile, unlike Type 2 hERG activators reported in the literature. It was not able to alter the cardiac rhythm, showing no proarrhythmic effect and being devoid of the chronotropic one, without even weakening the force of the cardiac contraction. The (R,S)-8 inotropic EC₅₀ value is one order of magnitude higher than that of mexiletine. Furthermore, it showed neither vasorelaxant activity on guinea pig aortic strips nor spasmolytic effect on guinea pig ileum smooth muscle, all these results together confirming a safe cardiovascular and intestinal profile. Due to its overall profile, (R,S)-8 may be considered a good starting point for the development of a novel congeneric series of hERG openers to treat both congenital and drug-induced forms of LQTS. The possible absence of unintended cardiovascular and nonvascular effects paves the way for the study of these mexiletine derivatives in in vivo models of LQTS.

4 | EXPERIMENTAL

4.1 | Chemistry

4.1.1 | General methods

Chemicals were purchased from Sigma-Aldrich or Lancaster in the highest quality commercially available. Solvents were RP grade unless otherwise indicated. Yields refer to purified products and were not optimized. The structures of the compounds were confirmed by routine spectrometric analyses. Only spectra for compounds not previously described are given. Melting points were determined on a Gallenkamp melting point apparatus in open glass capillary tubes and are uncorrected. ¹H NMR and ¹³C NMR spectra were recorded on either a Varian VX Mercury spectrometer operating at 300 and 75 MHz for ¹H and ¹³C, respectively, or an Agilent 500 MHz

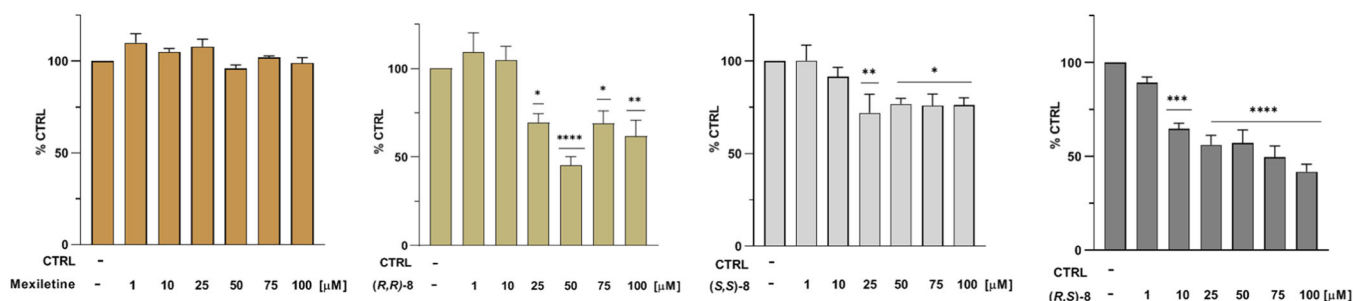


FIGURE 7 Viability of SH-SY5Y cells in the presence of mexiletine, (*R,R*)-, (*S,S*)-, and (*R,S*)-8. The cells were incubated for 24 h with the indicated compounds in the range of concentration 1–100 μM . Viability was performed with the 3-(4,5-dimethylthiazol-2-yl)-2,5-diphenyltetrazolium bromide (MTT) test and shown as means \pm SD, each performed in triplicates and referred to untreated control cells (CTRL, 100% values, in the absence of compounds). Statistical significance was calculated using a one-way analysis of variance (ANOVA) followed by Dunnett's test (GraphPad Prism version 5); * $p < 0.05$, ** $p < 0.01$, *** $p < 0.001$, **** $p < 0.0001$.

operating at 500 and 125 MHz for ^1H and ^{13}C , respectively, using CDCl_3 as solvent, unless otherwise indicated. Chemical shifts are reported in ppm relative to the residual nondeuterated solvent resonance: CDCl_3 , δ 7.26 (^1H NMR) and δ 77.3 (^{13}C NMR). J values are given in Hertz. Enantiomeric excess (ee) values were determined by chiral HPLC with an Agilent chromatograph (model 1100), equipped with a diode array detector, on a Daicel Chiralpak IA column. Electron ionization mass spectroscopy spectra were recorded on a Hewlett-Packard 6890–5973 MSD gas chromatograph/mass spectrometer at low resolution. The molecular ion is given as $[\text{M}]^+$. Elemental analyses were performed on a Eurovector Euro EA 3000 analyzer, and the data for C, H, and N were within ± 0.4 of theoretical values. Optical rotations were measured on a PerkinElmer Mod 341 spectropolarimeter; concentrations are expressed in $\text{g } 100 \text{ mL}^{-1}$, and the cell length was 1 dm; thus, $[\alpha]_{20}^{\text{D}}$ values are given in units of $10^{-1} \text{ deg cm}^2 \text{ g}^{-1}$. Chromatographic separations were performed on silica gel columns (Kieselgel 60, 0.040–0.063 mm, Merck). Thin layer chromatography (TLC) analyses were performed on precoated silica gel on aluminum sheets (Kieselgel 60 F254, Merck). TLC plates were visualized under UV light. The purity of the final compounds was determined by elemental analysis.

The InChI codes of the investigated compounds, together with some biological activity data, are provided as Supporting Information.

4.1.2 | Compound characterization

(+)-(*R*)-*tert*-Butyl [1-(1-hydroxypropan-2-yl)carbamate [(+)-(*R*)-2]

1.0 g (13.3 mmol) of (*R*)-alaninol [(*-*)-(*R*)-1] was dissolved in a mixture of 16 mL of 1 M NaOH and 20 mL of tetrahydrofuran (THF) and kept in an ice bath. A solution of BOC_2O (3.48 g, 16.0 mmol) in THF (10 mL) was then added dropwise and the mixture was stirred at 0°C for 30 min, then at room temperature overnight. All the reaction steps were performed in the darkness. After the evaporation of THF under vacuum, the aqueous phase was made acidic with 2 M HCl and extracted three times with ethyl acetate (EtOAc). The combined

organic phases were dried over Na_2SO_4 and concentrated under vacuum to give 2.7 g of a colorless oil which was crystallized from $i\text{Pr}_2\text{O}$ /hexane giving 2.09 g (90%) of white crystals: mp $58\text{--}59^\circ\text{C}$ ($i\text{Pr}_2\text{O}$ /hexane); $[\alpha]_{\text{D}}^{20} = +10.0$ (c 2, CHCl_3), lit.^[53] $+7.4$ (c 1, CHCl_3); GC-MS (70 eV) m/z (%) 144 ($\text{M}^+ - 31$, 45), 57 (100). Spectroscopic data were in agreement with those reported in the literature.^[53]

(*-*)-(*S*)-*tert*-Butyl [1-(1-hydroxypropan-2-yl)carbamate [(*-*)-(*S*)-2]

Prepared via the above reaction starting from (+)-(*S*)-1. Yield: 86%; white crystals; mp $58\text{--}59^\circ\text{C}$ ($i\text{Pr}_2\text{O}$ /hexane); $[\alpha]_{\text{D}}^{20} = -9.8$ (c 2, CHCl_3). Spectroscopic and spectrometric data were in agreement with the *R* isomer.

(+)-(*R*)-*tert*-Butyl [1-(2,6-dimethylphenoxy)propan-2-yl]carbamate [(+)-(*R*)-3]

1.0 g (5.7 mmol) of (+)-(*R*)-2, 1.04 g (8.6 mmol) of 2,6-dimethylphenol, and 2.25 g (8.6 mmol) of triphenylphosphine were dissolved in dry THF (27 mL) under N_2 atmosphere. A solution of 1.70 g of diisopropyl azodicarboxylate (8.6 mmol) in 13 mL of dry THF was then added dropwise. The mixture was stirred at room temperature for 24 h. The solvent was evaporated under vacuum giving a yellow oil purified by column chromatography on silica gel (EtOAc/hexane 1:9) to give 1.0 g (63%) of a white solid: mp $68\text{--}70^\circ\text{C}$ ($i\text{Pr}_2\text{O}$ /hexane), lit.^[54] $69\text{--}70^\circ\text{C}$; $[\alpha]_{\text{D}}^{20} = +20.0$ (c 0.5, CHCl_3), lit.^[54] $+22.2$ (c 1, CHCl_3); ^1H NMR (300 MHz): δ 1.38 (d, $J = 6.4$ Hz, 3H), 1.46 (s, 9H), 2.26 (s, 6H), 3.69 (dd, $J = 8.8, 3.5$ Hz, 1H), 3.76–3.80 (m, 1H), 3.99 (br s, 1H), 4.88 (brs, 1H), 6.91 (dd, $J = 8.8, 6.4$ Hz, 1H), 7.00 (d, $J = 7.0$ Hz, 2H); ^{13}C NMR (125 MHz): δ 16.1 (2C), 17.9 (1C), 28.4 (3C), 46.7 (1C), 74.1 (1C), 79.3 (1C), 124.0 (1C), 128.9 (2C), 130.8 (2C), 155.1 (1C), 155.4 (1C); GC-MS (70 eV) m/z (%) 279 (M^+ , <1), 122 (100).

(*-*)-(*S*)-*tert*-Butyl [1-(2,6-dimethylphenoxy)propan-2-yl]carbamate [(*-*)-(*S*)-3]

Prepared via the above reaction starting from (*-*)-(*S*)-2. Yield: 64%; $[\alpha]_{\text{D}}^{20} = -13.8$ (c 0.8, CHCl_3). Spectroscopic and spectrometric data were in agreement with those reported for the *R* isomer.

(-)-(R)-1-(2,6-Dimethylphenoxy)propan-2-amine [(-)-(R)-4]

0.9 g (3.2 mmol) of (+)-(R)-3 were dissolved in a mixture of 3.2 mL (44.9 mmol) of trifluoroacetic acid and CH₂Cl₂ (10 mL), then the mixture was stirred at room temperature for 4 h. After the evaporation of CH₂Cl₂ under vacuum, the residue was taken up with EtOAc and extracted with 2 M HCl. The aqueous phase was in turn made alkaline with 6 M NaOH and extracted three times with EtOAc. The combined organic phases were dried over Na₂SO₄ and concentrated under vacuum to give 0.400 g (70%) of a colorless oil: [α]_D²⁰ = -2.4 (c 2.0, MeOH), lit.^[55] -2.7 (c 4.7, CHCl₃); IR (KBr): 3364, 3293 (NH₂), 1203 (ArO) cm⁻¹. Spectrometric and spectroscopic data were in agreement with those reported in the literature.^[55,56]

(+)-(S)-1-(2,6-Dimethylphenoxy)propan-2-amine [(+)-(S)-4]

Prepared via the above reaction starting from (-)-(S)-3. Yield: 94%. [α]_D²⁰ = +2.6 (c 3, CHCl₃), lit.^[55] +2.5 (c 4.9, CHCl₃). Spectroscopic and spectrometric data were in agreement with those of the R-isomer.

(-)-(R,R)-1,3-Bis[1-(2,6-dimethylphenoxy)propan-2-yl]urea [(-)-(R,R)-8]

Method A: To a mixture of (-)-(R)-7 (0.46 g, 2.2 mmol), diphenylphosphoryl azide (0.90 g, 3.3 mmol) and Et₃N (1 mL, 7.2 mmol), a solution of 0.40 g (2.2 mmol) of (-)-(R)-4 in 30 mL of dioxane was added. The reaction mixture was kept under reflux for 18 h. After the evaporation of dioxane under vacuum, the residue was taken up with EtOAc, washed with 2 M HCl, then 2 M NaOH. The organic layer was dried over Na₂SO₄ and concentrated under vacuum to give 0.60 g of a white solid which was recrystallized from toluene/hexane to give 0.140 g (16%) of a white solid.

Method B: 0.35 g of (-)-(R)-4 (1.9 mmol) was dissolved in 10 mL of CH₃CN, then 0.166 g (1.0 mmol) of CDI was added and the mixture was stirred at room temperature for 18 h. After the evaporation of the solvent under vacuum, the residue was taken up with EtOAc and washed with 2 M HCl. The organic layer was dried over Na₂SO₄ and concentrated under vacuum to give 0.35 g of a white solid which was recrystallized from toluene/hexane. Yield: 77%; mp 203–205°C (toluene/hexane); [α]_D²⁰ = -6.2 (c 1, CHCl₃); ee 99% (HPLC: Chiralpak IA, flow rate 0.8 mL/min, eluent 80:20 hexane/EtOH. Supporting Information: Figures S1 and S2); IR (KBr): 3328 (NH), 1626 (C=O) cm⁻¹; ¹H NMR (300 MHz): δ 1.38 (d, J = 6.4 Hz, 6H), 2.24 (s, 12H), 3.69 (dd, J = 8.8, 3.5 Hz, 2H), 3.80 (dd, J = 8.8, 3.5 Hz, 2H), 4.16–4.17 (m, 2H), 4.96 (brs, 2H), 6.88–6.99 (m, 6H); ¹³C NMR (125 MHz): δ 16.3 (4C), 18.2 (2C), 46.2 (2C), 74.8 (2C), 123.8 (2C), 128.9 (4C), 130.7 (4C), 154.8 (2C), 157.2 (1C); HRMS *m/z* calcd for C₂₃H₃₂N₂O₃: 407.2305 ([M+Na]⁺); found 407.2304; Anal. Calcd for (C₃₂H₃₂N₂O₃·0.25 H₂O): C, 71.01; H, 8.42; N, 7.20; Found: C, 71.36; H, 8.19; N, 7.21.

(+)-(S,S)-1,3-Bis[1-(2,6-dimethylphenoxy)propan-2-yl]urea [(+)-(S,S)-8]

Prepared via the above reaction (Method B) starting from (+)-(S)-4. Yield: 90%; mp 203–205°C (toluene/hexane); [α]_D²⁰ = +6.7 (c 1,

CHCl₃); ee 99% (HPLC: Chiralpak IA, flow rate 0.8 mL/min, eluent 80:20 hexane/EtOH. Supporting Information: Figures S1 and S2). Anal. Calcd for (C₃₂H₃₂N₂O₃·0.66H₂O): C, 69.67; H, 8.47; N, 7.06. Found: C, 69.80; H, 8.03; N, 7.29. Spectroscopic and spectrometric data were in agreement with those reported for the RR isomer.

(R,S)-1,3-Bis[1-(2,6-dimethylphenoxy)propan-2-yl]urea [(R,S)-8]

0.179 g of (-)-(R)-4 (1.0 mmol) were dissolved in 15 mL of CH₃CN, then 0.162 g (1.0 mmol) of CDI was added and the mixture was stirred at room temperature for 5 h. Then, a solution of (+)-(S)-4 (0.179 g, 1.0 mmol) in CH₃CN (15 mL) was added dropwise, and the stirring was continued for 18 h at room temperature. After the evaporation of the solvent under vacuum, the residue was taken up with EtOAc and washed with 2 M HCl. The organic phase was dried over Na₂SO₄ and concentrated under vacuum to give 0.300 g of a white solid which was recrystallized from toluene/hexane. Yield: 78%; mp 186–188°C (toluene/hexane); IR (KBr): 3328 (NH), 1626 (C=O); ¹H NMR (300 MHz): δ 1.36 (d, J = 6.6 Hz, 6H), 2.26 (s, 12H), 3.69 (dd, J = 9.2, 4.0 Hz, 2H), 3.78 (dd, J = 9.2, 4.0 Hz, 2H), 4.13–4.19 (m, 2H), 5.03 (d, J = 7.9 Hz, 2H), 6.92 (dd, J = 8.6, 5.9 Hz, 2H), 7.00 (d, J = 7.3 Hz, 4H); ¹³C NMR (125 MHz): δ 16.1 (4C), 18.3 (2C), 46.5 (2C), 75.2 (2C), 124.0 (2C), 128.9 (4C), 130.8 (4C), 154.9 (2C), 157.6 (1C). Anal. Calcd for (C₃₂H₃₂N₂O₃·0.66H₂O): C, 69.67; H, 8.47; N, 7.06; Found: C, 69.51; H, 8.05; N, 7.12.

4.2 | Pharmacology

4.2.1 | Electrophysiological recordings

Human embryonic kidney (HEK) 293 cells were plated in a 6 cm Petri dish and transiently transfected using Effectene Transfection Reagent (Qiagen) with 1 μg pmCherry-N1-hERG-WT plasmid and incubated at 37°C and 5% CO₂. After 24 h the cells were split and seeded to perform electrophysiological recordings in the bath solution containing (in mM): 140 NaCl, 5 KCl, 1 MgCl₂, 2 CaCl₂, 10 HEPES, 10 glucose (pH 7.4 with NaOH). All ureas were tested to a final concentration of 25 μM. The I_{Kr} inhibitor E4031 (Sigma-Aldrich) was employed at the final concentration of 50 nM. The following intracellular solution (in mM): 130 KCl, 1 MgCl₂, 10 HEPES, 10 EGTA, 5 MgATP (pH 7.2 with KOH) was used to fill the patch-clamp glass pipettes (WPI) pulled by a P-97 puller (Sutter Instruments). hERG currents were recorded at room temperature in voltage-clamp-mode by the patch-clamp technique in whole-cell configuration. The patch-clamp amplifier was a Multiclamp 700B (Axon Instruments), the AD/DA converter was a DigiDadata 1322 A (Axon Instruments) connected to a personal computer running pClamp software (Version 9.2, Axon Instruments) used for data acquisition and analysis of the traces and Origin6.1 software for the Boltzmann fitting to obtain the half-point (V_{0.5}) and slope factor (k) for channel activation and inactivation. All the data were tested by two-tailed Student's paired *t* test. The significance level was considered at *p* < 0.05.

4.2.2 | Ex vivo functional studies

Guinea pigs of either sex (200–400 g) obtained from Charles River (Calco) were used. The animals were housed according to the ECC Council Directive regarding the protection of animals used for experimental and other scientific purposes (Directive 2010/63/EU of the European Parliament and of the Council). All procedures followed the guidelines of the animal care and use committee of the University of Bologna (Bologna, Italy). The ethical committee authorization was reported and numbered as “Protocol PR 21.79.14” by the Comitato Etico Scientifico for Animal Research Protocols according to D.L. vo 116/92.

Cardiac parameters (inotropy and chronotropic effects), antiarrhythmic effect, and spasmolytic activities on vascular and non-vascular smooth muscle (aorta and ileum respectively) of compounds were tested as previously described.^[19]

4.2.3 | Statistical analysis

Data were analyzed using Student's *t* test and are presented as mean \pm S.E.M. Since the drugs were added in a cumulative manner, the difference between the control and the experimental values at each concentration was tested for a *p* value < 0.05. The potency of drugs defined as EC₅₀ and IC₅₀ was evaluated from log concentration-response curves (Probit analysis using Litchfield and Wilcoxon)^[50] in the appropriate pharmacological preparations.

4.3 | Cell viability assay

4.3.1 | Chemicals and reagents

Dulbecco's modified Eagle's medium high glucose (DMEM), fetal bovine serum (FBS), penicillin, L-glutamine, streptomycin, and trypsin were purchased by Euroclone; MTT was provided from Sigma. SH-SY5Y cells were purchased from the American Type Culture Collection (ATCC).

4.3.2 | Cell viability on neuroblastoma SH-SY5Y

Immortalized human neuroblastoma SH-SY5Y cell line was cultured in DMEM containing 4.5 g/L D-glucose and non-essential amino acids, supplemented with 10% heat-inactivated FBS, 1% L-glutamine 200 mM, 100 U/mL penicillin and 100 μ g/mL streptomycin at 37°C in an atmosphere of 5% CO₂. At confluence 80%–90%, the cells were harvested and seeded at a density of 4×10^4 cells/well in a 96-well plate for 24 h, to approximately 70%–80% confluency. After this time, the culture medium was replaced by fresh medium containing the compounds (R,R)-**8**, (S,S)-**8**, and (R,S)-**8** used in the range of concentration from 0 to 100 μ M, respectively. The cells were treated for 24 h at 37°C in 5% CO₂ with the indicated concentrations of the

compounds and after the cell viability was tested by MTT [3-(4,5-dimethylthiazol-2-yl)-2,5-diphenyl tetrazolium bromide] assay as reported by Rullo et al.^[57] Absorbance values at 570 nm were measured using a multilabel plate counter Victor3 V (PerkinElmer), with dimethyl sulfoxide medium as the blank solution. Cells in DMEM alone represented negative control. Triplicate cultures were set up for each concentration of the tested compounds and each experiment was repeated three times. For each compound, IC₅₀ value was determined \pm SD.

4.4 | Crystallographic analysis

4.4.1 | General

X-ray diffraction powder data were collected at room temperature by a Rigaku RINT2500 diffractometer operating in transmission mode at Cu K α radiation ($\lambda = 1.540560 \text{ \AA}$). Samples were put on a glass capillary and spun during data collection. Data were collected in the 2θ range from 5° to 80°.

Crystal structure determination was performed by EXPO software,^[58] a package capable of carrying out the following steps: (a) determination of unit-cell parameters and identification of space group; (b) structure solution by direct methods and/or real-space approach; (d) structure model refinement by the Rietveld method.^[59] The first low-angle well-defined peaks in the experimental diffraction pattern were selected and actively used for indexing via N-TREOR09^[60] and DICVOL04^[61] programs embedded in EXPO. The space group determination was determined on the evaluation of the systematic absences.

The structures were solved with a real-space method based on the simulated annealing algorithm implemented in EXPO. The starting models were assembled using the sketching facilities of ACD/ChemSketch^[62] and the geometry optimization was achieved by the program MOPAC2016.^[63] The simulated annealing algorithm was run 100 times under Linux workstation in default mode and in parallel calculation over 20 CPUs. The solutions with the lowest cost function value were selected. The criterion to accept the solutions was also based on the soundness of crystal packing. The solutions obtained by the direct-space method were also confirmed by direct methods.

Density-functional theory (DFT) geometry optimization with Quantum ESPRESSO^[64] was only performed on hydrogen atoms to improve their positions. The structures derived were refined by the Rietveld method, considering the following variables: scale factor (1), lattice parameters (3 for (S,S)-**8** and 4 for (R,S)-**8**), atomic positions (84), isotropic thermal factors (3), peak-shape parameters (10), background parameters (17), and peak shift parameters (3). Restraints were applied to bond distances to stabilize the refinement (a total of 68 conditions for (S,S)-**8** and 29 for (R,S)-**8**). All H atoms bonded to C atoms were treated as riding under the constraint on atomic displacement parameters $U_{\text{iso}}(\text{H}) = 1.2 \cdot U_{\text{iso}}(\text{C})$. The peak shape was modeled using the Pearson VII function. The atomic displacement parameters were refined isotropically and constrained to have the

same value for atoms of the same chemical species. The correctness of the geometry of the refined molecules was confirmed when it was compared with the MOGUL^[65] average distances and angles.

To validate the refined crystal structures, they were subjected to periodic, solid-state calculations performed by Quantum ESPRESSO, an ab initio quantum-mechanical program employing plane waves and DFT to simulate the properties of solids. The following execution parameters were used: PBE potentials from the SSSP Efficiency PBE (version 1.1) library,^[66] an optional cut-off controlling the accuracy of the calculations set to 60 Ry, k-point spacing was 0.15 Å⁻¹, van der Waals interactions were corrected through a Grimme's D3 dispersion correction.^[67] Atomic-coordinate-only optimization of (R*,R*)-1,3-bis [1-(2,6-dimethylphenoxy)propan-2-yl]urea structures were performed using the experimental cell parameters and atomic positions obtained from Rietveld refinement.^[68] Crystal structures were visualized by using the Mercury program^[69] and were deposited on the CCDC database.

4.4.2 | Data availability

X-ray Crystallographic Information files for (S,S)-8 and (R,S)-8 are supplied as independent Supporting Information files. The crystal structures have been deposited on the Cambridge Crystallographic Data Centre via www.ccdc.cam.ac.uk/data_request/cif [CCDC 2209758 for (S,S)-8 and CCDC 2209759 for (R,S)-8].

4.5 | Molecular docking

4.5.1 | General

Induced-fit docking (IFD) simulations were performed on the cryo-EM structure of hERG (PDB code: 5VA1.^[70] In the first step, the retrieved.pdb file and the ligands were pretreated using the tools Protein Preparation Wizard (PPW)^[71] and LigPrep,^[72] respectively. These tools are available from the Schrödinger suite and allow to generate files suitable for simulation. In particular, PPW pretreats the.pdb file by adding missing hydrogen atoms, reconstructing incomplete side chains, assigning the ionization states at physiological pH, and setting the orientation of any misoriented group (N and O atoms as well as H residues). Furthermore, such a tool allows us to remove water molecules, optimize the hydrogen bond network, and perform a restrain minimization using the OPLS2005^[73] force field. LigPrep generates all the tautomers and ionization states at a pH value of 7.0 ± 2.0. Before starting the simulations, we selected the interaction region between the ligands and the hERG channel. In particular, we selected a cubic grid with an edge of 10 Å for the inner box and of 30 Å for the outer box, centered on the residues G628 and S631, in accordance with the available literature.^[27] Based on the IFD protocol, initial docking simulations were performed using the Glide standard precision (SP) mode, mutating G628 and S631 to alanine and scaling the van der Waals radii to 0.70. In the next step, up to 20 generated ligand–protein complexes, with the mutated residues

restored, were refined operating on residues within a maximum distance of 5 Å from each ligand pose and then minimized via the Refinement module of Prime, a tool available in the Schrodinger Suite 2022-1. Finally, each ligand was redocked to the obtained protein conformation using the extra precision (XP) protocol, the generated poses were ranked based on the obtained IFD scores and analyzed by visual inspection.

4.5.2 | MM-GBSA calculations

Following a protocol reported elsewhere,^[74] all the IFD complexes were subjected to MM-GBSA calculations.^[75] This protocol allowed us to estimate the binding free energies (ΔG) between protein and ligands.


ACKNOWLEDGMENTS

This work was supported by Fondazione Telethon—Italy (Grant # GGP19134) financed to Prof. Silvia G. Priori.

CONFLICT OF INTEREST STATEMENT

The authors declare no conflicts of interest.

ORCID

Maria Maddalena Cavalluzzi  <http://orcid.org/0000-0002-3402-8170>

Benny Danilo Belviso  <http://orcid.org/0000-0003-2880-1064>

Giovanni Lentini  <https://orcid.org/0000-0001-7079-5994>

REFERENCES

- [1] A. K. Ghosh, M. Brindisi, *J. Med. Chem.* **2020**, *63*, 2751.
- [2] I. Gallou, *Org. Prep. Proced. Int.* **2007**, *39*, 355.
- [3] J. Regan, S. Breitfelder, P. Cirillo, T. Gilmore, A. G. Graham, E. Hickey, B. Klaus, J. Madwed, M. Moriak, N. Moss, C. Pargellis, S. Pav, A. Proto, A. Swinamer, L. Tong, C. Torcellini, *J. Med. Chem.* **2002**, *45*, 2994.
- [4] A. Jagtap, N. Kondekar, A. Sadani, J.-W. Chern, *Curr. Med. Chem.* **2017**, *24*, 622.
- [5] J. M. Vega-Perez, I. Perinàn, M. Argandona, M. Vega-Holm, C. Palo-Nieto, E. Burgos-Morón, M. López-Lázaro, C. Vargas, J. J. Nieto, F. Iglesias-Guerra, *Eur. J. Med. Chem.* **2012**, *58*, 591.
- [6] E. Goffin, D. Lamoral-Theys, N. Tajeddine, P. de Tullio, L. Mondin, F. Lefranc, P. Gailly, B. Rogister, R. Kiss, B. Pirotte, *Eur. J. Med. Chem.* **2012**, *54*, 834.
- [7] J. Lan, L. Huang, H. Lou, C. Chen, T. Liu, S. Hu, Y. Yao, J. Song, J. Luo, Y. Liu, B. Xia, L. Xia, X. Zeng, Y. Ben-David, W. Pan, *Eur. J. Med. Chem.* **2018**, *143*, 1968.
- [8] O. C. Okpareke, W. Henderson, J. R. Lane, S. N. Okafor, *J. Mol. Struct.* **2020**, *1203*, 127360.
- [9] C. Brullo, F. Rapetti, O. Bruno, *Molecules* **2020**, *25*, 3457.
- [10] D. Gnocchi, S. Kapoor, P. Nitti, M. M. Cavalluzzi, G. Lentini, N. Denora, C. Sabbà, A. Mazzocca, *J. Mol. Med.* **2020**, *98*, 179.
- [11] D. Gnocchi, M. M. Cavalluzzi, G. F. Mangiatordi, R. Rizzi, C. Tortorella, M. Spennacchio, G. Lentini, A. Altomare, C. Sabbà, A. Mazzocca, *ChemMedChem* **2021**, *16*, 2121.
- [12] P. Zhou, J. Babcock, L. Liu, M. Li, Z. Gao, *Acta Pharmacol. Sin.* **2011**, *32*, 781.
- [13] M. C. Sanguinetti, *Curr. Opin. Pharmacol.* **2014**, *15*, 22.
- [14] S. Viskin, *Lancet* **1999**, *354*, 1625.

- [15] T. Jin, B. Hu, S. Chen, Q. Wang, X. Dong, Y. Zhang, Y. Zhu, Z. Zhang, *Front. Pharmacol.* **2018**, *9*, 577.
- [16] G. Milani, M. M. Cavalluzzi, C. Altamura, A. Santoro, M. Perrone, M. Muraglia, N. A. Colabufo, F. Corbo, E. Casalino, C. Franchini, I. Pisano, J.-F. Desaphy, A. Carrieri, A. Carocci, G. Lentini, *ChemMedChem* **2021**, *16*, 3588.
- [17] A. Catalano, A. Carocci, M. M. Cavalluzzi, A. Di Mola, G. Lentini, A. Lovece, A. Dipalma, T. Costanza, J.-F. Desaphy, D. Conte Camerino, C. Franchini, *Arch. Pharm.* **2010**, *343*, 325.
- [18] M. M. Cavalluzzi, G. Lentini, A. Lovece, C. Bruno, A. Catalano, A. Carocci, C. Franchini, *Tetrahedron Lett.* **2010**, *51*, 5265.
- [19] M. Roselli, A. Carocci, R. Budriesi, M. Micucci, M. Toma, L. Di Cesare Mannelli, A. Lovece, A. Catalano, M. M. Cavalluzzi, C. Bruno, A. De Palma, M. Contino, M. G. Perrone, N. A. Colabufo, A. Chiarini, C. Franchini, C. Ghelardini, S. Habtemariam, G. Lentini, *Eur. J. Med. Chem.* **2016**, *121*, 300.
- [20] A. Catalano, A. Carocci, G. Lentini, I. Defrenza, M. Maddalena Cavalluzzi, C. Franchini, *Drug Metab. Lett.* **2012**, *6*, 124.
- [21] S. G. Priori, O. Bonazzi, M. Facchini, T. Varisco, P. J. Schwartz, *Am. J. Cardiol.* **1987**, *60*, 1068.
- [22] S. G. Priori, C. Napolitano, P. J. Schwartz, *Arch. Mal. Coeur Vaiss.* **1996**, *89*, 1185.
- [23] A. Mazzanti, R. Maragna, A. Faragli, N. Monteforte, R. Bloise, M. Memmi, V. Novelli, P. Baiardi, V. Bagnardi, S. P. Etheridge, C. Napolitano, S. G. Priori, *J. Am. Coll. Cardiol.* **2016**, *67*, 1053.
- [24] A. Mazzanti, R. Maragna, C. Napolitano, S. G. Priori, *J. Am. Coll. Cardiol.* **2017**, *69*, 248.
- [25] W. Zhu, A. Mazzanti, T. L. Voelker, P. Hou, J. D. Moreno, P. Angsutararux, K. M. Naegle, S. G. Priori, J. R. Silva, *Circ. Res.* **2019**, *124*, 539.
- [26] P. J. Schwartz, S. G. Priori, E. H. Locati, C. Napolitano, F. Cantù, J. A. Towbin, M. T. Keating, H. Hammoude, A. M. Brown, L.-S. K. Chen, T. J. Colatsky, *Circulation* **1995**, *92*, 3381.
- [27] R. Gualdani, M. M. Cavalluzzi, F. Tadini-Buoninsegni, G. Lentini, *Biophys. Chem.* **2017**, *229*, 62.
- [28] M. M. Cavalluzzi, P. Imbriaci, R. Gualdani, A. Stefanachi, G. F. Mangiatordi, G. Lentini, O. Nicolotti, *Drug Discov. Today* **2020**, *25*, 344.
- [29] E. G. Chalina, L. Chakarova, D. T. Staneva, *Eur. J. Med. Chem.* **1998**, *33*, 985.
- [30] A. Ranise, F. Bondavalli, P. Schenone, M. Angrisani, M. Lisa, R. Marrazzo, E. Marmo, *Farmaco Sci.* **1988**, *43*, 79.
- [31] E. Mariani, F. Bondavalli, P. Schenone, G. Ciarallo, R. Spadaro, G. De Marco, G. D'angelo, E. Marmo, *Farmaco Sci.* **1982**, *37*, 438.
- [32] A. Ranise, F. Bondavalli, E. Mariani, P. Schenone, E. Lampa, L. Giordano, C. Vacca, E. Marmo, *Farmaco Sci.* **1983**, *38*, 884.
- [33] M. Longobardi, A. Bargagna, P. Schenone, D. De Santis, M. Angrisani, E. Marmo, *Farmaco Sci.* **1987**, *42*, 491.
- [34] M. Longobardi, A. Bargagna, P. Schenone, D. De Santis, M. Angrisani, E. Marmo, *Farmaco Sci.* **1987**, *42*, 691.
- [35] E. Mariani, F. Bondavalli, P. Schenone, A. Ranise, A. Marfella, R. De Carlo, G. M. Matera, E. Maramo, *Farmaco Sci.* **1982**, *37*, 36.
- [36] A. Carocci, A. Catalano, F. Turi, A. Lovece, M. M. Cavalluzzi, C. Bruno, N. A. Colabufo, M. Contino, M. G. Perrone, C. Franchini, G. Lentini, *ChemMedChem* **2016**, *11*, 93.
- [37] K. J. Padiya, S. Gavade, B. Kardile, M. Tiwari, S. Bajare, M. Mane, V. Gaware, S. Varghese, D. Harel, S. Kurhade, *Org. Lett.* **2012**, *14*, 2814.
- [38] J. P. Terhorst, W. L. Jorgensen, *J. Chem. Theory Comput.* **2010**, *6*, 2762.
- [39] V. S. Bryantsev, T. K. Firman, B. P. Hay, *J. Phys. Chem. A* **2005**, *109*, 832.
- [40] A. C. Legon, D. J. Millen, *Chem. Soc. Rev.* **1987**, *16*, 467.
- [41] C. Janiak, *J. Chem. Soc., Dalton Trans.* **2000**, *21*, 3885.
- [42] A. Adler, V. Novelli, A. S. Amin, E. Abiusi, M. Care, E. A. Nannenber, H. Feilotter, S. Amenta, D. Mazza, H. Bikker, A. C. Sturm, J. Garcia, M. J. Ackerman, R. E. Hershberger, M. V. Perez, W. Zareba, J. S. Ware, A. A. M. Wilde, M. H. Gollob, *Circulation* **2020**, *141*, 418.
- [43] T. M. Creanza, P. Delre, N. Ancona, G. Lentini, M. Saviano, G. F. Mangiatordi, *J. Chem. Inf. Model.* **2021**, *61*, 4758.
- [44] L. S. Grilo, P. A. Carrupt, H. Abriel, *Front. Pharmacol.* **2010**, *22*, 137.
- [45] M. Yan, P. Fan, Y. Shi, L. Feng, J. Wang, G. Zhan, B. Li, *Int. J. Mol. Sci.* **2016**, *17*, 1648.
- [46] A. El Harchi, O. Brincourt, *J. Arrhythm.* **2022**, *38*, 554.
- [47] M. D. Perry, C. A. Ng, M. M. Mangala, T. Y. M. Ng, A. D. Hines, W. Liang, M. J. O. Xu, A. P. Hill, J. I. Vandenberg, *Cardiovasc. Res.* **2020**, *116*, 1434.
- [48] Y. P. Shi, Z. Pang, R. Venkateshappa, M. Gunawan, J. Kemp, E. Truong, C. Chang, E. Lin, S. Shafaattalab, S. Faizi, K. Rayani, G. F. Tibbits, V. E. Claydon, T. W. Claydon, *Am. J. Physiol. Heart Circ. Physiol.* **2020**, *319*, H251.
- [49] J. M. Kemp, D. G. Whittaker, R. Venkateshappa, Z. Pang, R. Johal, V. Sergeev, G. F. Tibbits, G. R. Mirams, T. W. Claydon, *J. Gen. Physiol.* **2021**, *153*, e202112923.
- [50] R. J. Tallarida, R. B. Murray, *Manual of Pharmacologic Calculations with Computer Programs*, 2nd ed., Springer-Verlag, New York **1987**.
- [51] G. W. Zamponi, J. Striessnig, A. Koschak, A. C. Dolphin, *Pharmacol. Rev.* **2015**, *67*, 821.
- [52] F. De Ponti, C. Giaroni, M. Cosentino, S. Lecchini, G. Frigo, *Pharmacol. Ther.* **1993**, *60*, 121.
- [53] S. Dey, S. K. Gadakh, B. B. Ahuja, S. P. Kamble, A. Sudalai, *Tetrahedron Lett.* **2016**, *57*, 684.
- [54] M. Nechab, L. El Bliidi, N. Vanthuyne, S. Gastaldi, M. P. Bertrand, G. Gil, *Org. Biomol. Chem.* **2008**, *6*, 3917.
- [55] A. Carocci, C. Franchini, G. Lentini, F. Loiodice, V. Tortorella, *Chirality* **2000**, *12*, 103.
- [56] N. Viswanadh, R. Velayudham, S. Jambu, M. Sasikumar, M. Muthukrishnan, *Tetrahedron Lett.* **2015**, *56*, 5269.
- [57] M. Rullo, M. Cipolloni, M. Catto, C. Colliva, D. V. Miniero, T. Latronico, M. de Candia, T. Benicchi, A. Linusson, N. Giacchè, C. D. Altomare, L. Pisani, *J. Med. Chem.* **2022**, *65*, 3962.
- [58] A. Altomare, C. Cuocci, C. Giacobazzo, A. Moliterni, R. Rizzi, N. Corriero, A. Falcicchio, *J. Appl. Crystallogr.* **2013**, *46*, 1231.
- [59] H. M. Rietveld, *J. Appl. Crystallogr.* **1969**, *2*, 65.
- [60] A. Altomare, G. Campi, C. Cuocci, L. Eriksson, C. Giacobazzo, A. Moliterni, R. Rizzi, P. E. Werner, *J. Appl. Crystallogr.* **2009**, *42*, 768.
- [61] A. Boultif, D. Louër, *J. Appl. Crystallogr.* **2004**, *37*, 724.
- [62] ACD/ChemSketch 5.0 (2003) for MS-Windows, Advanced Chemistry Development, Inc. Toronto, ON, **2003**. <http://www.acdlabs.com>
- [63] MOPAC2016, Version 18.305L, in: J. J. P. Stewart, *Stewart Computational Chemistry*, Colorado Springs, CO, USA. <http://OpenMOPAC.net/> (accessed: December 2021).
- [64] P. Giannozzi, S. Baroni, N. Bonini, M. Calandra, R. Car, C. Cavazzoni, D. Ceresoli, G. L. Chiarotti, M. Cococcioni, I. Dabo, A. Dal Corso, de S. Gironcoli, S. Fabris, G. Fratesi, R. Gebauer, U. Gerstmann, C. Gougoussis, A. Kokalj, M. Lazzeri, L. Martin-Samos, N. Marzari, F. Mauri, R. Mazzarello, S. Paolini, A. Pasquarello, L. Paulatto, C. Sbraccia, S. Scandolo, G. Sclauzero, A. P. Seitsonen, A. Smogunov, P. Umari, R. M. Wentzcovitch, *J. Phys. Condens. Matter.* **2009**, *21*, 395502.
- [65] I. J. Bruno, J. C. Cole, M. Kessler, J. Luo, W. D. S. Motherwell, L. H. Purkis, B. R. Smith, R. Taylor, R. I. Cooper, S. E. Harris, A. G. Orpen, *J. Chem. Inf. Comput. Sci.* **2004**, *44*, 2133.
- [66] G. Prandini, A. Marrazzo, I. E. Castelli, N. Mounet, N. Marzari, *NPJ Comput. Mater.* **2018**, *4*, 72.
- [67] S. Grimme, J. Antony, S. Ehrlich, H. Krieg, *J. Chem. Phys.* **2010**, *132*, 154104.
- [68] J. van de Streek, M. A. Neumann, *Acta Crystallogr. B Struct. Sci. Cryst. Eng. Mater.* **2014**, *70*, 1020.

- [69] C. F. Macrae, P. R. Edgington, P. McCabe, E. Pidcock, G. P. Shields, R. Taylor, M. Towler, J. van de Streek, *J. Appl. Crystallogr.* **2006**, *39*, 4532006.
- [70] W. Wang, R. MacKinnon, *Cell* **2017**, *169*, 422.
- [71] Schrodinger Release 2022: Protein Preparation Wizard; Epik, Schrodinger, LLC, New York, NY, 2022; Impact, Schrodinger, LLC, New York, NY; Prime, Schrodinger, LLC, New York, NY, 2022.
- [72] Schrodinger Release 2022: LigPrep, Schrodinger, LLC, New York, NY, 2022.
- [73] J. L. Banks, H. S. Beard, Y. Cao, A. E. Cho, W. Damm, R. Farid, A. K. Felts, T. A. Halgren, D. T. Mainz, J. R. Maple, R. Murphy, D. M. Philipp, M. P. Repasky, L. Y. Zhang, B. J. Berne, R. A. Friesner, E. Gallicchio, R. M. Levy, *J. Comput. Chem.* **2005**, *26*, 1752.
- [74] P. Delre, F. Caporuscio, M. Saviano, G. F. Mangiatordi, *Front. Chem.* **2020**, *8*, 594009.
- [75] S. Genheden, U. Ryde, *Expert Opin. Drug Discov.* **2015**, *10*, 449.

SUPPORTING INFORMATION

Additional supporting information can be found online in the Supporting Information section at the end of this article.

How to cite this article: G. Milani, R. Budriesi, E. Tavazzani, M. M. Cavalluzzi, L. B. Mattioli, D. V. Miniero, P. Delre, B. D. Belviso, M. Denegri, C. Cuocci, N. P. Rotondo, A. De Palma, R. Gualdani, R. Caliandro, G. F. Mangiatordi, A. Kumawat, C. Camilloni, S. Priori, G. Lentini, *Arch. Pharm.* **2023**, e2300116.
<https://doi.org/10.1002/ardp.202300116>